

Interferometric Angular Sensing for LISA

Jenna Bergevin¹
DePaul University, Chicago, IL

August 13, 2012

Abstract

The main goal of LISA is to detect gravitational waves. This cannot be done unless the external force noises are well understood. There are many external forces that cause noise in the position measurements of free falling test masses (TM). In distinguishing noise from a signal, we must have the ability to measure the small-force noise with high precision. To simulate free falling TM on Earth, we use torsion pendulums. Torque noise sources on the TM have been improved by replacing Tungsten with fused silica, however, the silica noise floor still cannot be resolved. This is due to the read-out noise of the autocollimator and gravitational reference sensor (GRS), which are used to measure the pendulum's angular motion. In order to reduce the readout noise, we are building an interferometer to measure their angular motion. Using high-speed piezo mirrors, we determine the precision of the interferometer. This instrument will be able to detect movements at nanoradian resolutions. Measuring gravitational waves is only possible if the noise caused by the instruments is known, and it is below the frequency range of the waves. Direct measurement of gravitational waves will give us the ability to 'see' the universe through non-electromagnetic waves, providing insight into the physics of our universe.

¹ Adviser: Bill Weber, University of Trento

Introduction

The University of Trento is the main site for investigating the force noise on the torsion pendulum test masses (TM) associated with the LISA and LISA Pathfinder missions. They found that hanging TM on fused silica fiber as opposed to Tungsten gives less torque noise. However, this noise floor with fused silica has not been reached. This is due, in part, to noise in the readouts that measure the angular position of the TM. Currently, the autocollimator and gravitational reference sensor (GRS) are used to measure the angular movement; the measurements are limited by noise in these instruments. This is illustrated in figure 1 where the black, dashed line shows the thermal noise floor.

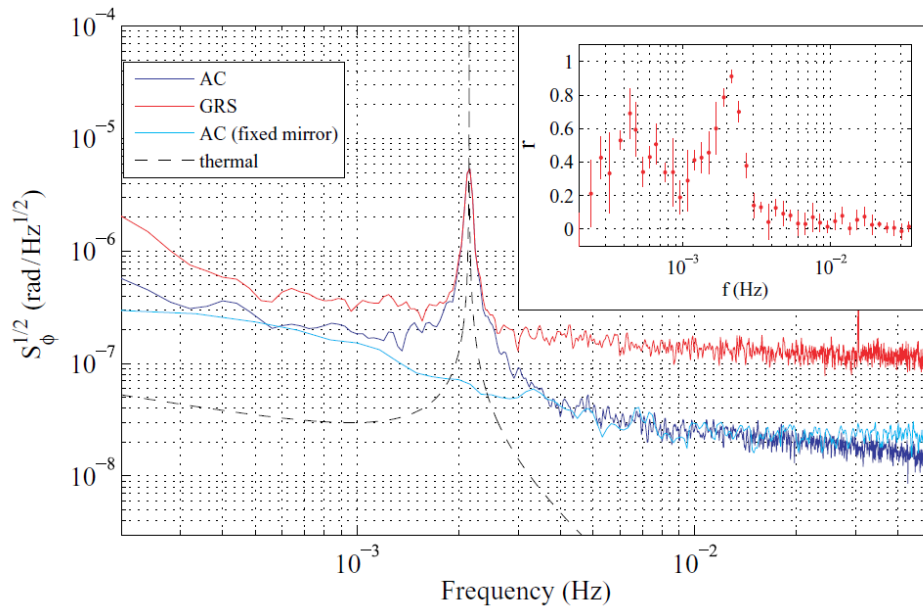


Figure 1. The angular noise versus frequency from an autocollimator and the GRS with a fused silica fiber, with the thermal noise floor. The peak indicates resonance. In the legend AC stands for autocollimator and GRS stands for gravitational reference sensor.

Clearly, the noise floor is not reached by either the autocollimator or the GRS. Although the cross-correlation analysis technique² demonstrates the ability to distinguish read-out noise from actual pendulum motion, the read-out noise still significantly contributes to the uncertainty in the force noise measurement. Therefore, we are building and implementing an interferometric angular sensor to have a higher precision angular measurement for the torsion pendulum.

The interferometer uses an infrared laser that initially splits the beam, and feeds both beams into acousto-optic modulators (AOM) to shift their frequencies. The frequencies differ by 1kHz, to allow a heterodyne detection at the photo diodes³. After the AOMs, the light beams are fed into optical fibers in order to traverse into the vacuum chamber.

² Carbone L *et al.* 2007 *Physics Review Letters* D75 042001

³ Heinzl G, AEI Hannover. 2002 *SMART-2 Interferometer* S2AEI TN 3010

Inside the vacuum chamber, the light from both beams is sampled, the reference beam goes straight to the photo diodes, and the measurement beam reflects of the TM before going to the photo diodes. This is shown in figure 2.

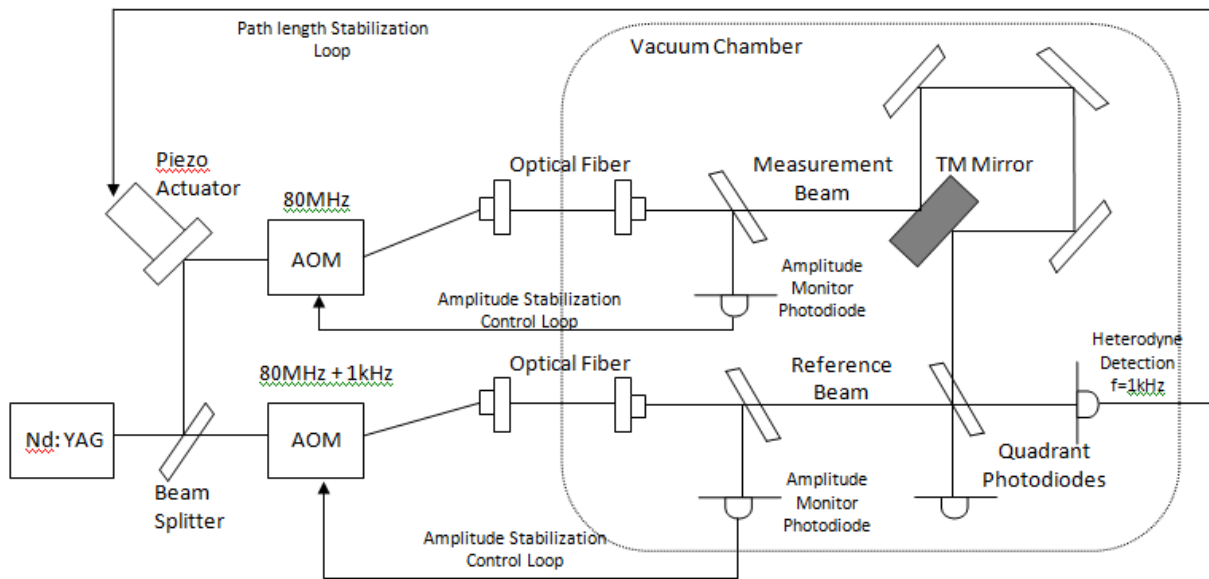


Figure 2. Layout of the angular interferometer.

The piezo actuator was unplugged and kept as a fixed mirror for the duration of this research.

Procedure

Initially, the interferometer was set up on an open-air optical bench as shown in figure 2 with the following changes: the piezo actuator as a fixed mirror, the TM mirror as a single fixed mirror (and excluding the three other mirrors), and single element photo diodes instead of quadrant photo diodes (QPD). This simplified version was used to align the light to reach the photo diodes. Once alignment was established, we began working towards the final set-up. The first effort was to switch from single element to QPDs.

A single element photo diode allows one to measure the total intensity of light on its surface. When the TM has an angular rotation, the light beam will change position. This movement cannot be detected by a single element photo diode because the total intensity does not depend on location (unless it moves off of the surface of the diode's surface). A QPD splits the surface into four detectors.

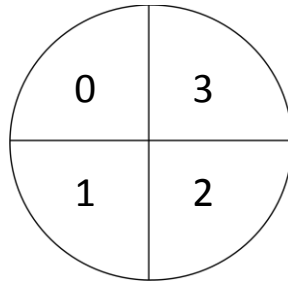


Figure 3. The surface of a QPD. The number labels correspond to the associated channel.

The quadrants are then referred to as channels, and the second QPD has channels 4-7 numbered in the same manner. With this set-up it is possible to detect the motion of the light beam by analyzing the differences between the signals. To implement the QPDs, we built an amplifier circuit for their signals. The circuit schematic is shown in figure 4.

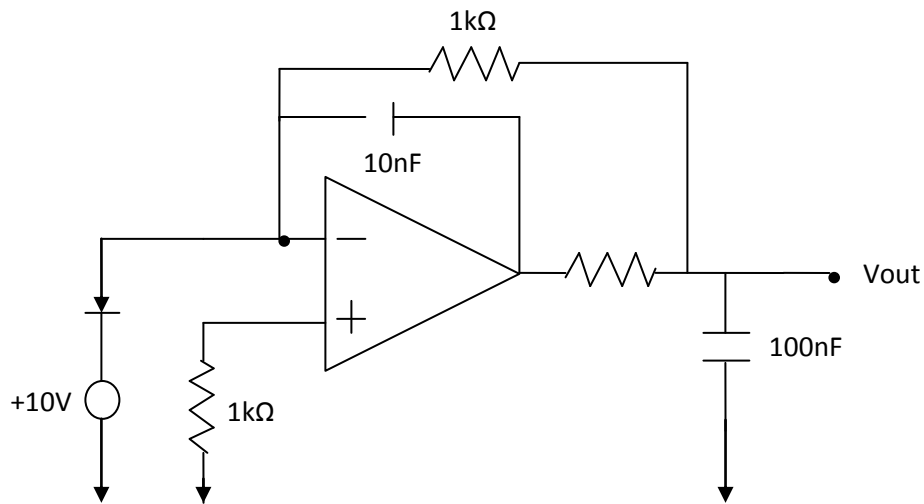


Figure 4. Circuit diagram for the QPD signal amplification.

This diagram is for one channel of the QPD. At first, we built the circuit on a bread board to make trouble shooting easier. This is shown in figure 5.

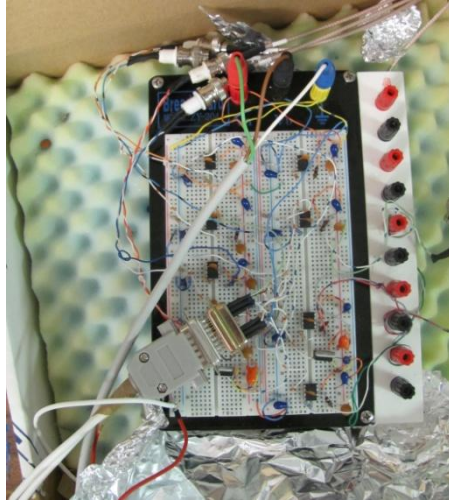


Figure 5. QPD circuitry on bread board.

The cable in the bottom left corner of figure 5 is the input from the interferometer. The outputs for 4 channels are shown on the top right, the other 4 are out of the picture on the right side.

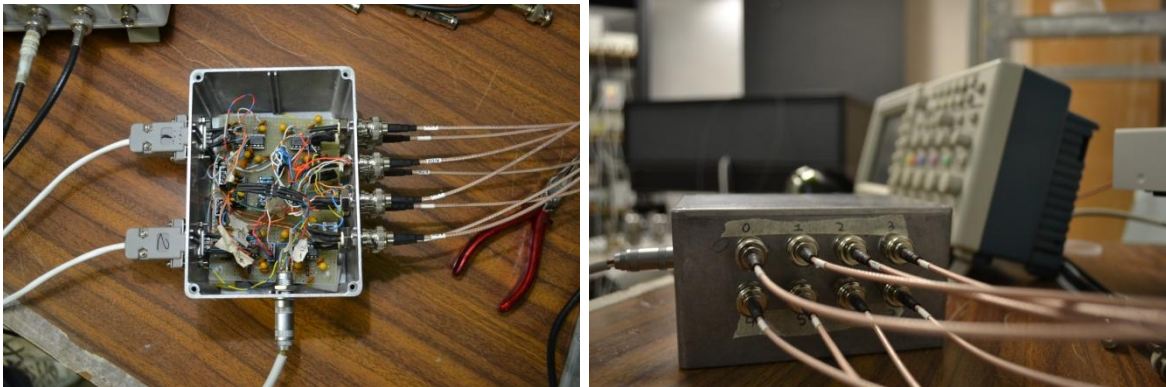


Figure 6. Finished circuit box for QPD amplifier.

The picture on the left shows the circuit box with the top taken off. The input cables from the interferometer are on the left, and the 8 channel outputs are on the right. The cable on the bottom is the power source. The picture on the right shows the output cables going into the computer. Again, the cable on the left of this picture is the power source. Once the circuitry was finished, and the QPDs were aligned, we were ready to begin measuring angles.

The fixed mirror in place for the TM mirror was replaced with a rotational stage. We attached a mirror to this device, which has the ability to move on in the x and y directions with a range on the order of milliradians at a resolution on the order of nanoradians. When it rotates on the y-axis, it moves the mirror in the x-direction, and we called this the alpha direction. Similarly, when it rotates on the x-axis, it moves the mirror in the y-direction, and we called this the beta direction.

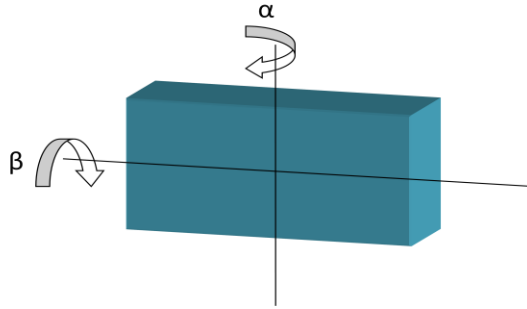


Figure 7. The directionality and labeling of the rotation of the stage.

The rotational stage works by inputting a voltage between 0V-10V in either direction, and this causes the stage to rotate. To calibrate the stage for the interferometer, we looked at the light intensity on the QPD. First, we modeled the intensity of the light using a simple Brownian model to imitate the Gaussian shape of the light

$$m(x, y) = \frac{1}{\sqrt{2\pi}\sigma} e^{-\frac{(x^2+y^2)}{2\sigma^2}}, \quad (1)$$

where σ is the 4-sigma area of the light. This value is determined by using an optical camera.

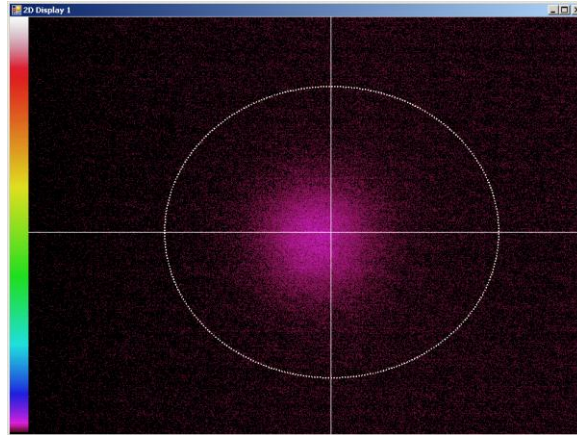


Figure 8. An image of the light beam taken with an optical camera. The 4-sigma area is outlined by the white circle.

The white circle is the 4-sigma area, and is used in Eq. (1). This function is then integrated to find the intensity

$$I_L(x) = \int_{-\infty}^x \int_{-\infty}^{\infty} m(x) dy dx$$

$$I_R(x) = \int_x^{\infty} \int_{-\infty}^{\infty} m(x) dy dx \quad (2)$$

where the subscripts refer to the left and right sides of the QPD. The definition of the change in angle is

$$2\alpha K = \frac{I_0+I_1-(I_2+I_3)}{I_0+I_1+I_2+I_3} \quad (3)$$

where α is the rotation angle, K is the calibration constant, and I stands for intensity with subscripts corresponding to the QPD channels. The right side is the normalized difference in intensity between the left and right sides of the QPD. Of course, this calculation can be done in the exact same way for the top and bottom halves of the QPD, as well as for the beta direction, and the second QPD. To simplify, we can rewrite the right hand side (refer to Eq. (3) and figure 3 for clarity),

$$2\alpha K_\alpha = \frac{I_L-I_R}{I_L+I_R}, \quad (4)$$

where the right hand side can be further simplified as

$$I_\Delta = \frac{I_L-I_R}{I_L+I_R}, \quad (5)$$

and finally Eq. (4) can be rewritten as

$$\begin{aligned} I_{\Delta 1} &= 2K_\alpha \alpha 1 \\ I_{\Delta 2} &= 2K_\alpha \alpha 2 \end{aligned} \quad (6)$$

where the subscripts represent calibrations around different values. The angles are not absolute, they are relative. We look for the change in angle, therefore, we use differences to solve for the calibration constant

$$I_{\Delta 2} - I_{\Delta 1} = 2K_\alpha \Delta\alpha. \quad (7)$$

Rearranging Eq. (7) makes it clearer,

$$K_\alpha = \frac{I_\Delta}{\Delta\alpha}, \quad (8)$$

where the 2 is absorbed by the calibration constant.

To measure the calibration constant we move the stage in small increments, and record the intensity from the QPDs at each step. By graphing the stage angle versus the intensity, we find the calibration constant as the slope of the graph.

The final change we made to the interferometer was to implement the vacuum chamber.

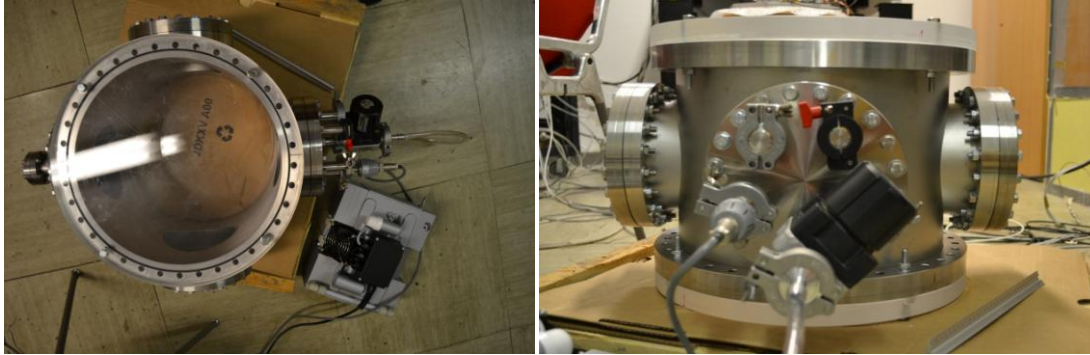


Figure 10. The vacuum chamber fully assembled from the top (left) and the side (right).

The lowest achieved pressure was around 1.5mBar. Inputs to the chamber include the pump, circuitry and optical fibers. The section of the interferometer that went into the vacuum chamber was reassembled on a smaller optical board, still with the rotational stage in place of the TM mirror.

Results & Discussion

The theoretical values for the calibration constant are given in table 1.

Theoretical	QPD1 (rad)	QPD2 (rad)
$K\alpha$	609	366
$K\beta$	431	259

Table 1. Theoretical values for the calibration constant. These values were recorded when one beam of light was blocked.

We noticed that the β direction gave us lower values. The second QPD also gives lower values; this is due to the length the light had to travel to reach this QPD. The longer distance the light had to travel decreased the intensity upon the surface of the QPD, resulting in consistently lower values than QPD1.

The measured values were found from the graph of the stage angle versus the output of the interferometer.

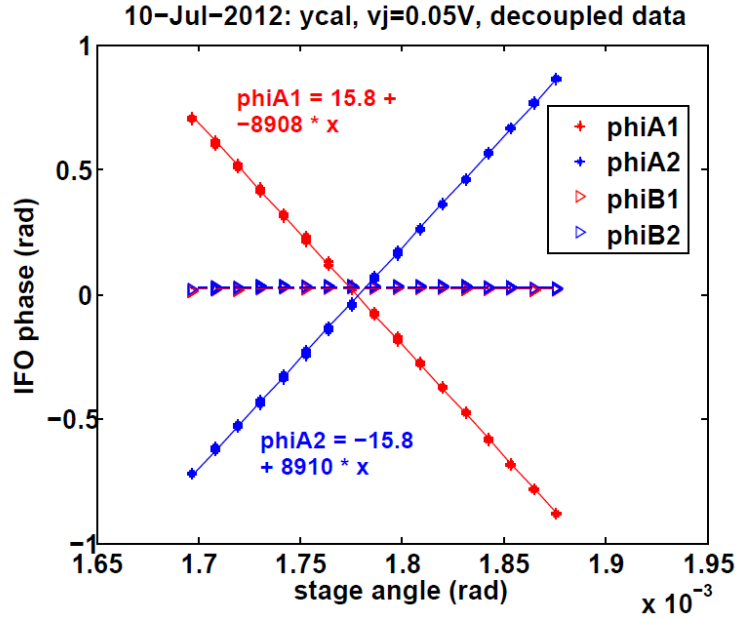


Figure 9. Stage angle versus interferometer output graph, the slope gives the calibration constant for y-axis. This data is taken when the light beams are recombined. In the legend, A corresponds to α , B to β , and the numbers indicate the proper photo diode. Corresponding values can be found in table 3.

The measured values are given in tables 2 and 3. There are values for one light beam blocked, and both light beams recombined.

Experimental	QPD1 (rad)	QPD2 (rad)
$K\alpha$	617	394
$K\beta$	423	264

Table 2. Measured values for the calibration constant. These values were calculated when one beam of light was blocked.

Interfered Beams	QPD1 (rad)	QPD2 (rad)
$K\alpha$	8909	8910
$K\beta$	6208	6195

Table 3. Measured values for the calibration constant. These values were calculated with the beams recombined, and correspond to figure 9.

Again, the β values are lower. Ultimately, we found that this is due to coupling in the rotational stage. When a voltage is applied to rotate the stage in the y-direction, the stage actually moves a small amount in the x-direction as well. The change in angle depends on two factors

$$\alpha = \frac{dx}{2L_1}, \quad (9)$$

where dx is the change in x , L is the length between the rotational stage and the detection at the photo diode, the subscript indicates the first photo diode, and there is a constant factor of one half. For the y -direction,

$$\beta = \frac{dx}{\sqrt{2}L_1}. \quad (10)$$

Again, dx is the change in x , and the constant value is smaller here. However, ideally there should be no movement in the x -direction when voltage is applied to the y -axis. Plugging Eq. (9 & 10) into Eq. (8) gives

$$K_\alpha = 2 \frac{L_1 I \Delta}{dx} \quad (11)$$

$$K_\beta = \sqrt{2} \frac{L_1 I \Delta}{dx}, \quad (12)$$

which gives the difference in the calibration constants. This can be seen by multiplying the K_β values in tables 1 and 2 by the factor of $\sqrt{2}$. We found this coupling first by experiment, and the factor of square root two is from the geometry of the interferometer. After we de-couple the data, we can use the calibration constants to solve for the change in angle. The vacuum measurements allow us to measure angular movements on the order of 50nrad. This is one power of ten larger than we strive for.

The angular phase noise without the vacuum section is shown below.

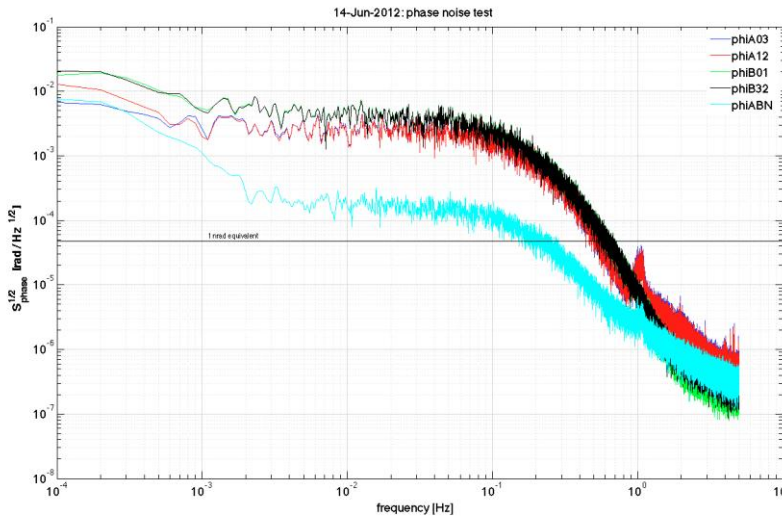


Figure 10. Angular phase noise in open air. In the legend, A corresponds to α , B to β , and the numbers indicate the channels. The teal color ABN is the difference between the x and y directions.

It can be seen that at frequencies between 10^0Hz and 10^{-1}Hz the noise increases. Comparing this to the phase noise with the vacuum chamber implemented, we saw two interesting differences.

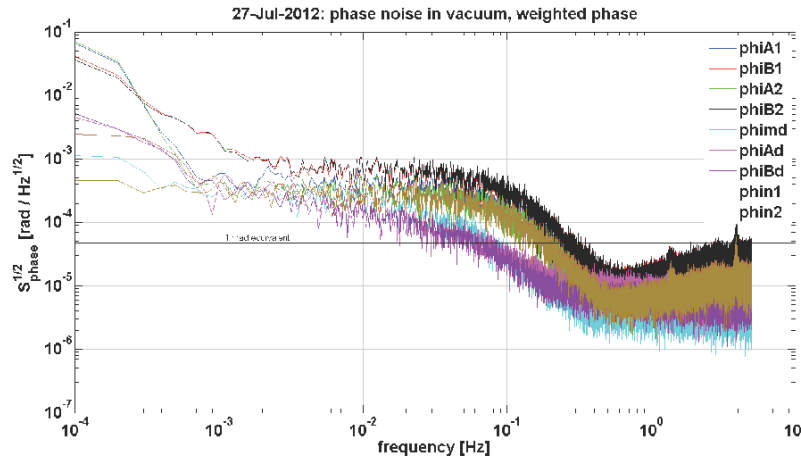


Figure 11. Angular phase noise in vacuum. In the legend, A corresponds to α , B to β , and the numbers indicate the channels. The phiAd and phiBd are the differences between α and β respectively.

First, with the vacuum, the noise begins to increase at lower frequencies. However, the noise at higher frequencies is also much higher than in open-air. This could be due to the vacuum pressure increasing during the time the measurement is taking place. Additionally, we found that the optical fiber cables are extremely sensitive. Slight movement in these cables can cause major distortion in the measured data.

A possible solution to the pressure increase is to keep the pump on during the measurement, and stifling the movement caused by it. As for the optical fibers, we must find a way of securing the fibers, and ensuring that the pump movement does not affect them.

Conclusion

To better understand the torque force noise on the torsion pendulum test mass, we built an interferometer to measure the angular motion. This was necessary because there is a high amount of noise due to the readouts of the autocollimator and gravitational reference sensor. Ultimately, the interferometer was able to detect angular movements with a resolution of 50nrad , which is one order of magnitude larger than our goal. Moving forward, we work towards increasing the effectiveness of the vacuum chamber and optical fiber cable stabilization to lower the noise and reach the level of detection near 5nrad resolution.

Future Work

Further work is necessary to de-bug the vacuum measurements. The first attempts should include securing the optical fiber cables, and keeping the vacuum pump constantly on. The latter approach would also need to take into account subduing the movement it causes, possibly by moving the pump into another room and feeding the

tube through a box of sand. Once the interferometer can resolve angular movements on the order of nanoradians, we will replace the rotational stage with the test mass pendulum. Lastly, we must record the total noise contributions from each component of the interferometer.

Acknowledgements

I would like to thank Bill Weber for the time and effort he put into getting me acclimated, giving me direction and answering all my questions and Hai-Bo Tu for his patience and guidance throughout the summer. Also, the Università di Trento for hosting me, the University of Florida and the NSF for funding my research experience.